Implementation of Tidbinbilla 70-m On-The-Fly mapping and Hydrogen radio recombination line early results

G. F. Wong[1,2]*, S. Horiuchi[3], J. A. Green[2,4], N. F. H. Tothill[1], K. Sugimoto[5], M. D. Filipovic[1]

[1] *Western Sydney University, Locked Bag 1797, Penrith 2751 NSW, Australia*
[2] *CSIRO Astronomy & Space Science, Australia Telescope National Facility, PO Box 76, Epping, NSW 2121, Australia*
[3] *CSIRO Astronomy & Space Science/NASA Canberra Deep Space Communication Complex, PO Box 1035, Tuggeranong ACT 2901, Australia*
[4] *SKA Organisation, Jodrell Bank Observatory, Lower Withington, Macclesfield SK11 9DL, UK*
[5] *National Astronomical Observatory of Japan, 2-21-1 Osawa, Mitaka, Tokyo 181-8588, Japan*

ABSTRACT

On-the-fly mapping of cm-wave spectral lines has been implemented at the the Tidbinbilla 70-m radio antenna. We describe the implementation and data reduction procedure and present new H92α radio recombination line maps towards Orion A and Sagittarius A. Comparison of the Orion A map to previous observations suggests that the lines arise largely from gas with electron density of 100–200 cm^{-3}. On-the-fly mapping is very efficient at generating large maps of bright lines (such as radio recombination lines), but will still yield strong efficiency gains for smaller maps of fainter lines, such as the ammonia inversion lines at the 1.3 cm wavelength.

Key words: Instruments: miscellaneous – ISM: Hii regions. – radio lines: ISM. – techniques: imaging processing

1 INTRODUCTION

The Deep Space Station 43 (DSS-43) is a 70-m single dish radio telescope that is part of the NASA Canberra Deep Space Communication Complex (CDSCC) located in the Australian Capital Territory (hereafter referred to as 'Tid-70m'). A small fraction of its time is devoted to radio astronomy and it is important to maximise the scientific return on this time. As such developments have been under way to implement On-The-Fly (OTF) mapping capabilities, to allow for an efficient survey option. Following the preliminary work of Young et al. (2013), we present full details of the implementation of OTF mapping at the telescope allowing for greater mapping efficiency. More efficient spatial mapping of the ammonia inversion transitions in the 17–27 GHz K-band is a strong driver of the implementation of OTF on the Tid-70m, but the technique may be used to map other radio lines, such as radio recombination lines (RRLs) that fall in the cm-wave bands. We used OTF mapping with Tid-70m to observe the H92α RRL at 8.3 GHz towards the prominent Galactic Hii region Orion A (Ori A) and the Galactic Centre feature Sagittarius A (Sgr A).

OTF mapping involves sampling the sky while the antenna is moving at a constant rate, rather than integrating at a discrete position on the sky, then moving to the next position. The technique is widely used by mm- and submm-wave telescopes to produce large-scale maps in molecular transitions and the greybody continuum, such as CO 3–2 mapping towards M 83 (Muraoka et al. 2009), maps of CO and 1.1 mm continuum emission towards Ori A (Shimajiri et al. 2011), and 90 GHz maps of star-forming clumps (Jackson et al. 2013). Detailed descriptions of the technique have been presented by Mangum et al. (2007) and Sawada et al. (2008). Implementation of OTF mapping at the Australia Telescope National Facility (ATNF) Mopra telescope has yielded several large mapping surveys (e.g. Wong et al. 2011; Jones et al. 2013; Braiding et al. 2015).

Peters et al. (2012) reviewed the physics of hydrogen RRL emission: the populations depart significantly from local thermodynamic equilibrium (LTE) over frequency ranges that depend on the electron density. Peters et al. consider ALMA and EVLA observations of compact high-density Hii regions, but also show that for the larger, less dense Hii regions that might be mapped with a single-dish telescope, non-LTE effects are important in the centimetre-wavelength range. Gordon & Sorochenko (2009) used a non-LTE analysis to show how the line brightness varies with frequency and electron density. We may therefore estimate the electron density from the frequency dependence of line brightness. The line brightness depends on electron temperature
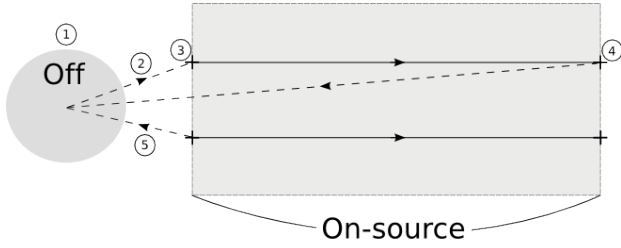
Figure 1. The sequence of steps in an OTF observation. The target region to be mapped is shown as a shaded rectangle. The solid line indicates telescope movement, starting and stopping at the crosshairs, during which the spectrometer is continuously sampling. The dashed line shows telescope movement without spectrometer sampling. In this example, every scan row is observed before making an OFF measurement, shown as a shaded circle.

and density, so RRL maps can be used to infer the structure of ionised gas (e.g. Jaffe & Pankonin 1978).

2   OBSERVING PROCESS

While many OTF scan patterns can be implemented, we have used the simplest, the raster (Fig. 1), which is optimised for mapping rectangular regions. Raster scanning moves the telescope on-source, 'ON', in a straight line, then offsets by a fraction of a beam, perpendicular to the scan direction, before moving the telescope in the opposite direction. An emission-free reference position, 'OFF', is also observed to correct for the bandpass. As the telescope moves across the source, the spectrometer samples data at regular intervals.

Our implementation is a variation of the raster geometry, where the order of observing on-source or reference position is flexible: an OFF can be observed before or after an ON, or after multiple ON scans (see §2.2 and 2.3 for details). Maps can be made in either ($\alpha \cdot \cos \delta_0$, δ) or ($a \cdot \cos e_0$, e) coordinate systems, with the scan direction parallel to either coordinate axis [1].

2.1   Software Architecture

The OTF observing mode was implemented on the control software AUTO_SPEC, a PERL based script that acts as an interface to the telescope and spectrometer. This software sends commands via two PERL modules: network monitor control (NMC.PM) and correlator (CORR.PM). These commands are sent to the antenna pointing control (APC) and the user interface (TKCOR) respectively. The NMC module interacts with NASA controlled modules of the telescope. The commands the NMC module sends are: setting position; offset; slew rate; stop and stow. The module also retrieves information on the current a and e coordinates, offsets, slew rate and supplementary information (temperature, pressure, humidity, wind speed, wind direction, precipitation and time). The antenna logs that are generated by the

---

[1] a, e are azimuth and elevation. δ_0 is the declination of the starting position of the observation. The longitudinal coordinates are referred to as cross-Dec and cross-El in the telescope control system.
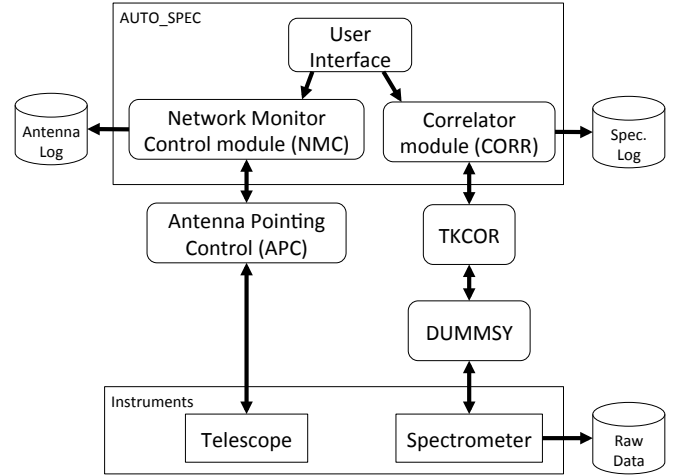

Figure 2. Schematic illustration of the telescope system. The rounded rectangles are processes involved with OTF, rectangles are individual instruments and cylinders represent data storage and files.

NMC module contain telescope commands and records of the position. The CORR module interacts with the user interface TKCOR, a PERL/TK module that is the interface of the process DUMMSY. DUMMSY sends commands to the physical correlator. Logs from the spectrometer are generated from CORR.PM. Fig. 2. is a schematic illustration of the architecture of the software control system.

2.2   Antenna

The commands to move the telescope come from the schedule file, setting the parameters of the observation, containing positional information for the reference position and starting position on source, time on source and frequency. Scanning axis and direction for on-source scanning are programmed into the control software AUTO_SPEC before observations begin. In a typical OTF mapping observation, where a reference position is taken, first, then a single on source observation:

(i) OTF mapping begins with integrating on an emission-free reference position;

(ii) the telescope slews to the start position of the target source;

(iii) the OTF scan starts with AUTO_SPEC commanding the telescope control to settle on the α and δ starting point before moving the telescope in a set direction at a constant rate with a timer starting;

(iv) the scan rate of the telescope is calculated based on the beam size, and sampling rate:

$$R = \frac{\theta_{int}}{t_{int}} = \frac{d\alpha}{dt} \cos \delta_0 \qquad (1)$$

(assuming scanning in $\alpha \cos \delta_0$), where R is the scanning rate of the telescope in degrees s^{-1}, θ_{int} is defined as θ_{FWHM}/n (n is the number of times to sample the beam, generally ≥ 3) and t_{int} is the number of seconds per integration;

(v) as the telescope continues to slew across the source, the antenna log samples the telescope's position in a and e every 15 seconds.

(vi) the telescope will be sent the command to stop when the timer matches the on source time in the schedule file;

(vii) once the telescope has stopped, the next line in the schedule file is read.

2.3 Spectrometer

The Tid-70m is equipped with a Parkes Multibeam correlator block [2]. OTF observations can use the full 64 MHz bandwidth with two polarisation products of up to 2048 channels for each polarisation. As the telescope is being driven, the spectrometer is integrating the spectra over a minimum time interval of three seconds. The data from the spectrometer are then written to an ATNF format file (RPFITS[3]) along with time stamps, positional information, frequencies and summary information of the observation. The summary information contains start and finish time, observation project number, source name, starting position in α and δ as well as a and e, number of Intermediate Frequencies (IFs), observed frequency, reference frequency and system temperature (T_{sys}/K). The spectrometer will only record the starting position of each row of the map into the spectrometer log file through the correlator module, and this starting position is derived from the schedule file, not the telescope encoders. The average position of each sample was therefore derived by cross-checking the NMC log against the spectrometer log, taking into account slew times and correlator delays. This was done by the python data processing scripts FILLOBSERVATORIES.PY[4] and FIXDIRECTION_V2.PY[5]. These scripts also adjust the sample positions (see section 2.4).

2.4 Data processing

Data processing of 70m-Tid OTF data uses the Common Astronomy Software Applications (CASA version 4.1 and 4.2; McMullin et al. 2007). The raw file (RPFITS) containing header information, tables and observation data is imported into CASA, with positions converted into radians. Correcting the position of each integration is based on converting the recorded velocity taken from NMC log into radians and compensating for the initial delay caused by the correlator. The scan rate (R), is then used to correct the position of each integration along the $\alpha \cos \delta_0$ axis:

$$\alpha_i = \alpha_0 + \frac{R}{\cos \delta_0} \cdot (t_i - t_0) \tag{2}$$

where α_0 and t_0 are the starting R.A. and time, and α_i and t_i are the R.A. and time of the current integration (δ_0 is the corresponding declination for α_0). The new positions are written into the scan table, as well as the recalculated a

[2] www.atnf.csiro.au/observers/tidbinbilla
[3] www.atnf.csiro.au/computing/software/rpfits.defn
[4] spacescience.uws.edu.au/~honours/Graeme_W/fillobservatories.py
[5] spacescience.uws.edu.au/~honours/Graeme_W/fixDirection_v2.py

and e for each new position. The antenna temperature T_A is obtained by bandpass correcting the raw spectrum:

$$T_A = T_{sys} \cdot \frac{ON - OFF}{OFF} \tag{3}$$

T_{sys} is the system temperature, ON is the on-source spectrum and OFF is the reference spectrum.

The schedule file contained a reference scan for each on-source scan; the SDCAL task in CASA assumes this format. Polynomial baseline subtraction can occur at this stage, or a continuum subtraction can be applied after the imaging stage is completed to preserve the continuum emission. Smoothing functions such as the Hanning function can also be applied if the target spectral line is narrow. Calibrated data are then exported into a measurement set (MS) format for the imaging stage, which creates a position-position-velocity cube using both circular polarisations. The gridding kernel is the default 2-D top-hat function with a 1-pixel width. Continuum subtraction from the image cube can be applied (if baseline subtraction was not applied to the spectra), through the specification of a line-free channel range, resulting in a continuum cube and emission line cube. The data cube can then be exported to FITS. The detailed CASA data reduction procedure is described in Appendix A.

3 TEST OBSERVATIONS

The HII region Ori A and Galactic centre source Sgr A were the targets for our test observations (Table 1). Observations were conducted under Tid-70m project T206, as part of the OTF development programme. Our test observations used the 8.2–8.6 GHz X-band receiver and recorded both circular polarisations with 64 MHz bandwidth, sampling at a quarter FWHM with the minimum three second intervals. The beam has FWHM $1.8'$, and individual scans (map rows) were spaced by $30''$ in Dec, while the telescope scanned along the $\alpha \cdot \cos \delta_0$ axis. A schedule file parameter set the time taken for the telescope to complete each scan: These observations used 120s-long scans with 30s integrations on the reference position. The Hanning function was not applied for the maps presented, as RRLs are broad spectral features, so Hanning is not required. Opacity correction was not applied to our maps, but attenuation due to opacity would be within 5% at the lowest elevation during the 8 GHz observations. There was no comparison to a flux calibrator source, but our observations agree within 10% with those of Cesarsky (1973).

Ori A and Sgr A were mapped with the same telescope scan speed of $-2.48 \, \mathrm{mdeg \, s^{-1}}$ along $\alpha \cdot \cos \delta_0$; converting the scan speed to α and using the minimum integration time of 3s, Ori A and Sgr A have cell sizes of $0.45'$ and $0.51'$ respectively along the scan direction, and $0.5'$ across the scan direction. Offsets caused by the delay of the spectrometer were between $0.30'$ and $0.60'$ for Ori A and $0.34'$ and $0.68'$ for Sgr A. The scan speed is taken from the NMC log which records telescope speed, and the integration time is taken from correlator logs (The negative scanning speed indicates that the telescope was moving in decreasing $\alpha \cdot \cos \delta_0$.). The effect of these corrections is to shift each scan row by a slightly different amount along the scan direction. The resulting Sgr A image has a continuum peak shifted to the position of Sgr A* compared to the uncorrected image which had a $2.5'$ offset from Sgr A*.

Table 1. Table showing the different sources observed, the date observed, the amount of time taken to observe, map size in arcmin, central position of the map and reference position.

| Region	Date Observed	Time Duration	Map Size (R.A. × Dec)	Map Size (Pixels)	Central map position R.A. (J2000) Dec (J2000)	Reference position R.A. (J2000) Dec (J2000)
Ori A	2013-09-24	2.4 h	$18.9' \times 17.5'$	42×36	05:35:19.2 −05:18:47.7	05:40:30.0 −05:16:16.0
Sgr A	2013-09-23	2.8 h	$20.4' \times 16.0'$	42×42	17:45:58.9 −28:58:22.1	17:55:00.0 −28:00:00.0
	2013-09-24	1.3 h	$20.4' \times 10.5'$	42×21	17:45:58.9 −28:43:28.3	17:55:00.0 −28:00:00.0
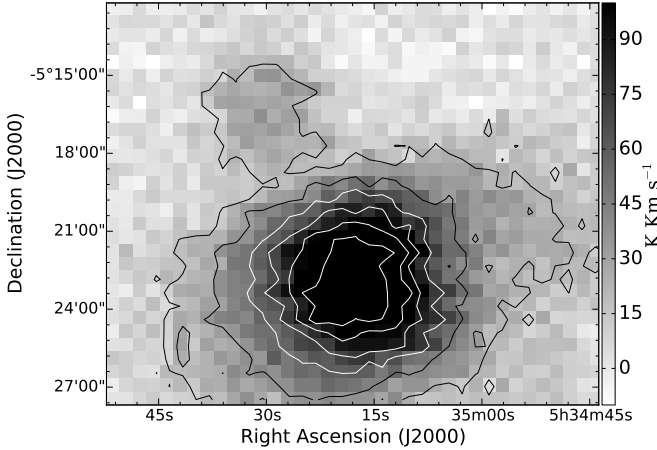
Figure 3. Integrated H92α emission map towards Ori A; contours at 20, 40, 60 ... 140 K km s^1.

Both sources were observed with channels of width 1.13 km s^{-1}. The Ori A integrated H92α emission map is shown in Fig. 3. Continuum subtraction was applied to the Ori A cube after the imaging process, as this correctly produced a flat spectrum. Sgr A was observed on two separate days; data from each day were processed separately before merging the datasets during the imaging stage. H92α integrated and channel maps towards Sgr A are shown in Figs. 4 and 5 respectively. While the data cube has a channel width of 1.13 km s^{-1}, the channel map in Fig. 5 uses a channel width of 15 km s^{-1}. Because of the complex emission structure of the region, an attempt was made to select a line-free channel range to create a polynomial to remove continuum emission from the spectra. Examining the attempted continuum subtraction, we see the Northern region with continuum emission successfully removed. However, around the Southern peak ($\delta < -28°55'$) broadband emission can still be seen. Continuum emission is still present within Figs. 4 and 5.

4 DISCUSSION

4.1 Orion A

Our data constitute the first fully-sampled single-dish RRL map of Ori A, though sparsely-sampled maps made up of selected beam positions have previously been published by Jaffe & Pankonin (1978) and by Peimbert et al. (1988); the RRL structure (Fig. 3) is similar to that seen in a
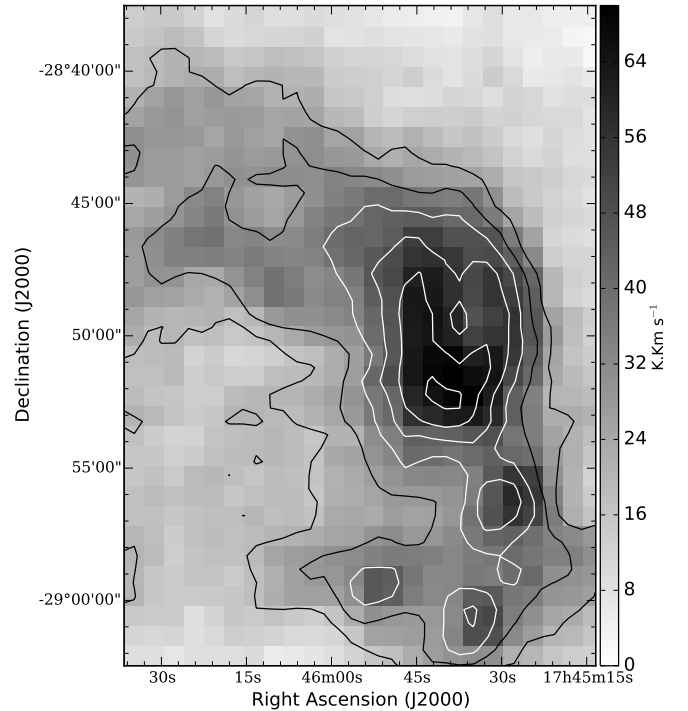
Figure 4. Integrated H92α emission map with incomplete continuum subtraction towards Sgr A; contours at 20, 30, 40 ... 70 K km s^{-1}.

23 GHz continuum map (resolution 42$''$, Wilson & Pauls 1984). Many hydrogen RRL transitions have been observed with single-dish telescopes towards Ori A, mostly towards similar positions, so that the beams overlap. Table 3 lists H(n)α RRL transitions observed towards positions close to the peak brightness that we observe in Ori A. The spectrum corresponding to the peak brightness in our H92α map (Fig. 6 and Table 2) may be compared to a previous observation of the same transition by Cesarsky (1973), which used the DSN Goldstone antenna, then 64 m in aperture, with beamwidth of 2.5$'$. No pointing coordinates are given, but the published line parameters (T$_A$ = 4.65 K, V$_{LSR}$ = −2.7±2 km s^{-1}, $\Delta\nu$ = 26±2 km s^{-1}), agree with our results (Table 2) within the error intervals, except for line amplitude; but even here, the discrepancy of 0.42 K is less than 10%.

Fig. 7 is replotted from Sorochenko (1965), with observational data points added by taking the line brightnesses from Table 3 divided by the emission measure of the HII region (EM of 4.0×10^6 cm^{-6} pc taken from McGee & Newton
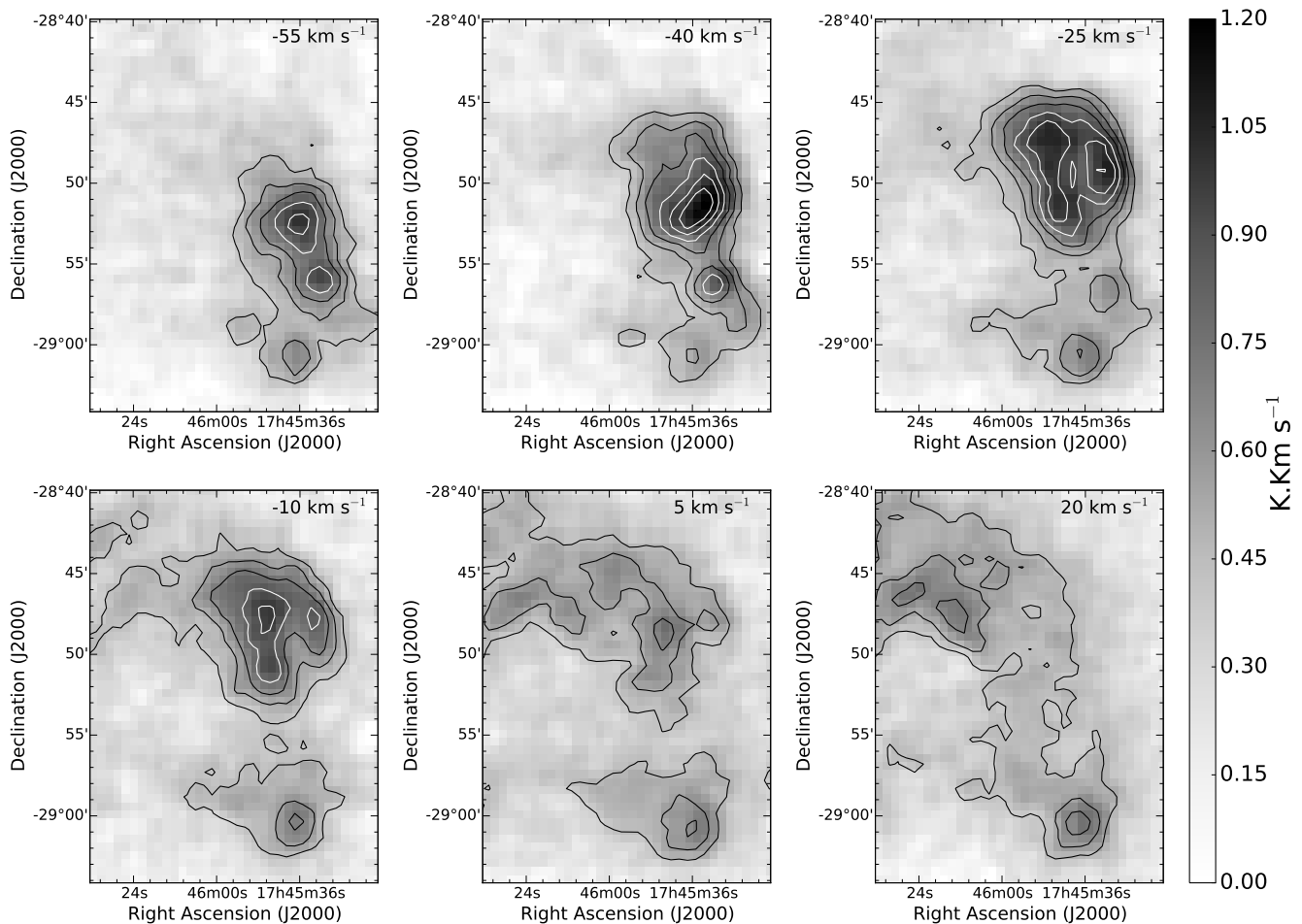
Figure 5. On-the-fly channel maps with incomplete continuum subtraction of H92α emission towards Sgr A; contours at 0.3, 0.45, 0.6. . . 1.2 K.

Table 2. Gaussian fits to sample H92α spectra.

Region	R.A. J2000	Dec J2000	V$_{LSR}$ (km s^{-1})	$\Delta\nu$ (km s^{-1})	T$_A$ (K)
Ori A	05:35:17.8	−05:22:15.0	−2.7±0.3	25.0±0.7	5.07±0.12
Sgr A	17:45:41.4	−28:52:14.9	−40.5±0.8	56.2±2.0	0.88±0.03

1981), and shows the variation of RRL brightness with electron density. All the lines denoted by pentagons are observed at similar positions, and the filled pentagon is the value taken from our map. Triangles denote observations with no position given. The model curves show that we should expect significant changes in the relative line brightnesses around 10 GHz as the electron density increases from 100 cm^{-3} to 1000 cm^{-3}. Observations at these frequencies therefore present an opportunity to probe the electron density directly through RRLs, and large-scale mapping of RRLs at these frequencies may allow us to map electron density structure.

The data points in Fig. 7 generally lie near the model curves for electron densities of 100 and 200 cm^{-3}. Points lying significantly away from these tracks are at an uncertain position (7.8 GHz) or an upper limit (24.5 GHz). Estimates of the electron density towards Ori A generally lie at least an order of magnitude higher: Smirnov et al. (1984) calculated an electron density of $(1\pm 0.3)\times10^4$ cm^{-3}, based on Stark broadening of RRLs, and García-Díaz & Henney (2007) suggest the electron density is generally around 2000 cm^{-3} throughout Ori A, based on optical spectroscopy.

García-Díaz & Henney (2007) found a layer of low-electron-density emission towards Ori A, lying in front of the main ionised region, and blueshifted. Fig. 7 shows that low-electron-density gas emits very strongly around 10 GHz, so it is possible that much of the H92α emission that we see arises in lower-density material. Wen & O'Dell (1995) modelled the dense layer of ionised material in Ori A as being
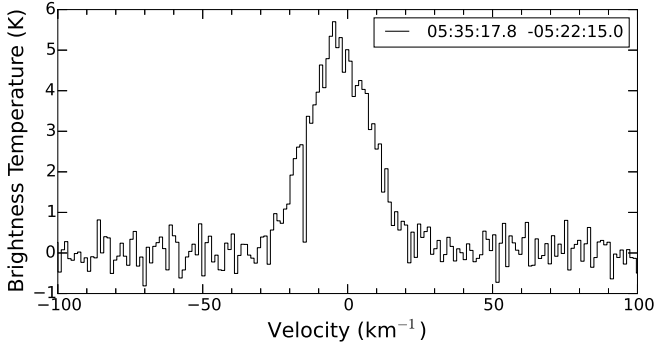
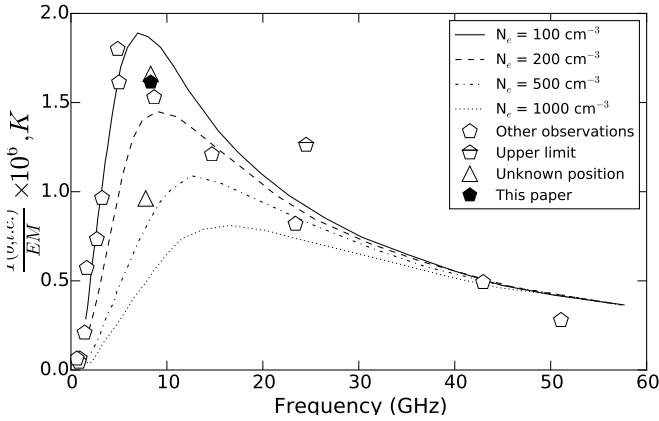**Figure 6.** H92α spectrum towards Ori A at the position of peak T_L (coordinates top right).

Figure 8. Sample H92α spectra towards Sgr A.

sion seen in the maps as broadband emission in the southern peak ($\delta < -28°55'$). However, we see a 'peanut' shape in our H92α map (Fig 4) similar to that seen by Pauls et al. (1976) in H85α (10 GHz, 1.3$'$ beam); our channel map (Fig 5) and the spectrum towards the emission peak (Fig. 8) are consistent with the finding of Pauls & Mezger that the dominant H109α (5 GHz, 2.6$'$ beam) emission occurs at $V_{LSR} \sim -40\,\mathrm{km\,s^{-1}}$.

Figure 7. Brightness temperature at the center of a line as a function of frequency (Sorochenko 1965), overlaid with peak antenna temperatures (Table 3) of Hydrogen RRLs towards Ori A observed at different frequencies.

0.1–0.2 pc thick, so the denser gas might account for less than half of the $4 \times 10^6\,\mathrm{cm^{-6}}$pc emission measure; hence there could be a large amount of low-density gas to generate the RRLs. To confirm this possibility, a full spatial analysis of RRLs across frequencies and comparison to continuum maps would be required, falling outside the scope of this paper.

4.2   Sagittarius A

Sgr A has been mapped interferometrically in the H92α RRL using the VLA (Zhao et al. 1993; Roberts & Goss 1993; Lang, Goss & Morris 2001; Lang, Goss & Wood 1997), but the high resolution of these maps rules out simple comparisons to our data.

Pauls et al. (1976) and Pauls & Mezger (1980) used the 100-m Effelsberg telescope to map H85α and H109α RRL emission towards the Sgr A region. Continuum subtraction was applied on the Sgr A data set, although due to the strong Sgr A non-thermal emission affecting the entire band profile, there still remains some continuum emis-
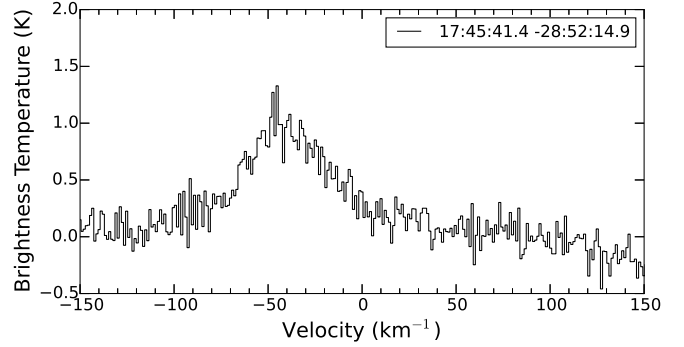
4.3   On-the-fly mapping on the 70-m

Our maps use a 30$''$ row spacing, more finely-sampled than the Nyquist row spacing criteria suggested by Mangum et al. (2007), resulting in oversampling of the rows. Our scan rate implies an oversampling factor (n_{os} in Eq. 10, Mangum et al. 2007) close to 1.5 for Sgr A and 2 for Ori A.

Mapping a region the size of Ori A (18.9$'$×17.5$'$ map) by position switching would take about 25 hours, an order of magnitude more than the time taken to map it with OTF (Table 1). The major contributor to the time requirement for position switching is the telescope motion overhead, as the telescope moves back and forth between the map position and the reference. From OTF mapping logs, each such movement takes 12–32 s, 25 s on average. Most of this time is required to accelerate, decelerate and settle the telescope, so it is likely not to be strongly dependent on the distance to the reference position. Because mapping of the bright hydrogen RRLs only requires a few seconds' integration (compared to the tens of seconds of movement overhead), RRL mapping probably gains the most efficiency from OTF.

The ammonia inversion transitions in the 17–27 GHz K-band are widely used to probe the temperature of cold dense gas; OTF may be used to map these lines. A 10$'$ × 10$'$ position-switching map with 60 s integration on-source per position, mapped at half-beam spacing will take $\sim$ 29 h and reach rms noise of $\sim$ 0.07 K. This sensitivity is likely to be useful for ammonia analysis. To map a similar area with OTF, spacing map rows by half a beam and sampling each row every third of a beam, using the minimum 3 s integration time, takes 1.4 hours, achieving an estimated rms noise of 0.3 K. Co-adding 12 repeated maps (taking into account that the OTF map is more densely sampled than the position-switched map), will yield an rms of $\sim$ 0.07 K in $\sim$ 17 hours, about 0.6 of the time required for the position-

Table 3. Table containing Hydrogen RRL transition, rest frequency, peak brightness temperature (T_A), beam efficiency, line brightness temperature corrected for beam efficiency (T_L) and available publications with single dish observation towards Ori A in the H$n\alpha$ RRL. The H109α T_L appears to be have already been corrected for beam efficiency (Jaffe & Pankonin 1978). The H64α T_L had already been corrected for beam efficiency and with a smaller beam than our observations (42″), the data point in Fig 7 is an upper limit (Wilson et al. 1997). Our 92α spectrum (R.A. 05:35:14.8, Dec. –05:22:32.4) is towards the overlap of the other H(n)α transitions.

Transition	Rest Frequency (GHz)	T_A (K)	η	T_L (K)	Reference
50	51.07	0.67	0.65	1.03	Hollis & Ulich (1977)
53	42.95	0.98	0.65 ± 0.05	1.97	Peimbert et al. (1988)
64	24.51	—	—	5.05	Wilson et al. (1997)
65	25.40	1.54	0.47	3.28	Churchwell et al. (1970)
76	14.69	2.95	0.70	4.21	McGee & Newton (1981)
91	8.67	4.28	0.70	6.11	Quireza et al. (2006)
92	8.31	4.65	0.70 ± 0.2	6.64	Cesarsky (1973)
92	8.31	4.57	0.70	6.53	This paper
94	7.79	2.04	0.53	3.85	Gordon & Meeks (1967)
109	5.01	—	0.65	6.45	Jaffe & Pankonin (1978)
110	4.87	5.40	0.75	7.20	Davies (1971)
126	3.24	2.70	0.70	3.86	McGee & Gardner (1968)
134	2.70	2.20	0.75	2.93	Zuckerman & Palmer (1970)
158	1.65	1.60	0.70	2.29	McGee et al. (1969)
166	1.42	0.56	0.67	0.84	Pedlar & Davies (1972)
192	0.92	0.17	0.67	0.25	Pedlar & Davies (1972)
198	0.84	0.10	0.55	0.18	Zuckerman & Ball (1974)
220	0.61	0.17	0.67	0.25	Pedlar & Davies (1972)

switching map. Each row of the OTF map takes 150 s, so the reference position is checked every 3.5 min; 4 min is the approximate maximum time between reference spectra at K-band. K-band observations will require opacity and gain-curve corrections for the corrected temperature scale (T_A^*) which is applied after importing into CASA. Smoothing using the Hanning function can be applied at a later stage.

For compact ammonia sources, observing efficiency can be increased by averaging the ends of the scan rows as an OFF spectrum in the data processing, removing the need for a reference scan. This approach will require reformatting the raw file to allow CASA to separate on-source spectra from OFF spectra for processing.

5 CONCLUSIONS

The 70-m Tidbinbilla radio telescope is now capable of on-the-fly (OTF) spectral line mapping. We have tested the new observing mode by mapping radio recombination line emission towards Orion A and Sagittarius A: Our data are consistent with published data towards these regions.

We have combined our measurement of the peak brightness towards Orion A with other measurements from the literature over a wide range of frequency, and plotted the line brightnesses over the theoretical curves of Sorochenko (1965). The line brightness measurements are most consistent with electron densities of 100–200 cm^{-3}, much lower than usual estimates of the electron density of the Orion nebula. This discrepancy may reflect the more efficient RRL emission from lower-density gas. Comparison of RRL brightness over a wide frequency range has the potential to constrain the electron density of large ionised regions, but this requires large-scale mapping to allow different beams to be compared as well as to analyse spatial structure. OTF mapping, which is highly efficient at mapping RRLs, can enable this analysis.

Because of the long times required for the Tid-70m to switch between source and reference, large maps of bright lines (such as RRLs) are very efficiently mapped by OTF, while smaller maps of fainter lines (requiring longer integration times) do not gain as much. At K-band, the requirement to go to a reference position every $\sim$ 4 min sets a limit to the mapping efficiency that can be achieved. Even so, maps of ammonia inversion transitions should be significantly more efficient using OTF.

REFERENCES

Balser D. S., Goss W. M., De Pree C. G., 2001, ApJ, 121, 371
Bell M. B., Avery L. W., MacLeod J. M., Vallee J. P., 2011, Ap&SS, 333, 377
Braiding C., et al. 2015, PASA, 32, 20

Cesarsky D. A., 1973, ApJ, 184, 397

Churchwell E., Mezger P., Reifenstein III E., Rubin R., Turner B., 1970, Aplett, 5, 157

Davies R. D., 1971, ApJ, 418, 479

García-Díaz M. T., Henney W. J., 2007, ApJ, 133, 952

Gordon M. A., Meeks M. L., 1969, ApJ, 149, 21

Gordon, M. A. & Sorochenko, R. L. 2009, Radio Recombination Lines. Springer Publishers Group, USA, NY

Hollis J. M., Ulich B. L., 1977, ApJ, 214, 699

Jackson J. M. et al., 2013, PASA, 30, 57

Jaffe D. T. Pankonin V., 1978, ApJ, 226, 869

Jones P. A., Burton M. G., Cunningham M. R., Tothill N. F. H., Walsh A. J., 2013, MNRAS, 433, 221

Lang C. C., Goss W. M., Morris M., 2001, ApJ, 121, 2681

Lang C. C. L., Goss W. M., Wood D. O. S., 1997, ApJ, 481, 1016

Lockman F. J., Brown R. L., 1975, ApJ, 201, 134

Mangum J. G., Emerson D. T., Greisen E. W., 2007, A&A, 474, 679

McGee R. X., Batchelor R. A., Brooks J. W., Sinclair M. W., 1969, AuJPhys, 22, 631

McGee R. X., Gardner F. F., 1968, AuJPhys, 21, 149

McGee R. X., Newton L. M., 1981, MNRAS, 196, 889

McMullin J. P., Waters B., Schiebel D., Young W., Golap K., 2007, ASP Conf. Ser, 376, 127

Muraoka K., et al, 2009, ApJ, 706, 1213

Pauls T., Downes D., Mezger P. G., Churchwell E., 1976, A&A, 46, 407

Pauls T., Mezger P. G., 1980, A&A, 85, 26

Pedlar A., Davies. R. D., 1972, MNRAS, 159, 129

Peimbert, M., Ukita N., Hasegawa T., Jugaku J., 1988, PASJ, 40, 581

Peters T., Longmore S. N., Dullemond C. P., 2012, MNRAS, 425, 2352

Quireza C, Rood R. T., Balser D. S., Bania T. M., 2006, ApJS, 165, 228

Roberts D. A., Goss W. M., 1993, ApJS, 86, 113

Sawada T., et al., 2008, PASJ, 60, 445

Shimajiri Y. et al., 2011, PASJ, 63, 105

Smirnov, G. T., Sorochenko R. L., Pankonin V., 1984, A&A, 135, 116

Sorochenko R. L., 1965, Trudy Fiz. Inst., P. N. Lebedeva Akad. Nauk USSR 28, 90

Wen Z., O'Dell C. R., 1995, ApJ, 438, 784

Wilson, T. L.; Filges L., Codella C., Reich W., Reich P., 1997, A&A, 327, 1177

Wilson T. L., Pauls T., 1984, A&A, 138, 225

Wong T., 2011, ApJ, 197, 16

Young T., Horiuchi S., Green J. A., Jerjen H., 2013, MNRAS, 435, 3568

Zhao J.-H. et al., 1993, ApJ, 418, 235

Zuckerman B., Ball J. A., 1974, ApJ, 190, 35

Zuckerman B., Palmer P., 1970, A&A, 4, 244

APPENDIX A: CASA PROCESS STEPS

The raw file from Tid-70m OTF is in RPFITS format, imported by the CASA task SDSAVE. SDLIST creates a list summary of the observations. A plot of pointings before position correction can be generated by SDPLOT using parameter POINTING in argument PLOTTYPE. An experimental script (FIXDIRECTION_V2.PY; see section 2.3), corrects the OTF pointings using the velocity taken from the NMC log files. a and e are calculated for the new positions with the ASAP RECALC_AZEL() method on the scantable. Opacity correction can be applied on the scantable through the ASAP OPACITY method. SDPLOT is used again to confirm adjustments made

to the pointings. Calibration is completed by task SDCAL, with the parameter CALMODE set to QUOTIENT. Baseline subtraction can be applied through the command SDBASELINE. Spectra can be smoothed through the SDSMOOTH task, using the Hanning function by default. To view the spectra, the task SDPLOT is used, setting parameter PLOT TYPE to GRID. After calibration is completed, SDSAVE exports the data into a measurement set (MS) file.

CASA task SDIMAGING generates the position-position-velocity cube, setting parameter DOCHANNEL to TRUE. The expandable parameters of DOCHANNEL are also required: START, STEP and NCHAN. START gives the beginning of the cube in the velocity axis; STEP is the value for each channel; NCHAN is the number of channels in the velocity range. Values for START, STEP and NCHAN are in units of SPECUNIT. CELL is the size of each pixel: Values for the OTF maps are spacing between each scan (in Dec) and cell size along the scan derived by converting the scan rate (from the NMC log) from milli degree s^{-1} to arc seconds s^{-1}, by the number of seconds per integration. Image size is set by parameter IMSIZE, based on the number of samples taken per scan and number of scans across source. SDIMAGING by default averages both polarisations during the imaging process.

If baseline subtraction has not been applied, continuum subtraction can be used through task IMCONT. A line free channel range must be specified, before running the command. Integrated intensity images can be created by using the task IMMOMENTS. The image can be exported to a FITS file by task EXPORTFITS.

This paper has been typeset from a TeX/LaTeX file prepared by the author.